FUDMA Journal of Engineering and Technology
ISSN: 3092-9385
https://fjet.fudutsinma.edu.ng/index.php/fjet/
Volume 2, Issue 2, 2026, 186-203

Design, Simulation, and 3D Printing of a Lightweight Drone Frame for Farm Monitoring

Abdulkareem BELLO[1*], Saleh S. LUKMAN[2], Tasie M. CHIZE[3], Yusuf O. ADEIZA[4], Chibuzor A. OKAFOR[5], Abdullahi O. YAKUBU[6]

[1*,2,5,6]Mechanical Engineering Department, Ahmadu Bello University, Zaria, Nigeria
[3]Department of Mechanical Engineering, Rivers State University, Nkpolu Oroworukwo Port Harcourt, Rivers State, Nigeria
[4]Department of Mechanical Engineering, Confluence University of Science and Technology, Osara, Kogi State, Nigeria

[1*]ogabello2002@yahoo.com, [2]sslukman01@gmail.com, [3]martin.tasie@gmail.com, [4]adeiza007yus@gmail.com, [5]caokafor96@gmail.com, [6]abdullahiomeizayakubu@gmail.com

Abstract
This research presents the design, simulation, and fabrication by fused deposition modelling (FDM) 3D printing of a lightweight quadcopter frame for agricultural monitoring, aimed at developing a cost-effective and structurally efficient alternative to commercial drone frames. The project integrates Computer-Aided Design (CAD) in SolidWorks 2023 and Finite Element Analysis (FEA) in ANSYS Workbench 2024 to predict the frame's structural and thermal performance before fabrication. The drone frame geometry was reverse-engineered and scaled down from the DJI (Da-Jiang Innovations) Agras T100 platform, with adjustments to fit the mission requirements of low-altitude crop monitoring. Acrylonitrile Butadiene Styrene (ABS), of density 1.02 g/cm³ and tensile yield strength 40 MPa, was selected as the fabrication material due to its balance of strength, low density, and cost-effectiveness. Static, modal, steady-state thermal and thermal-stress simulations were carried out under a thrust load of 25 N per motor arm, a solar heat flux of 1000 W/m², an ambient temperature of 40 °C and a convective heat transfer coefficient of 20 W/m²K. The analysis returned a maximum equivalent (von Mises) stress of 2.4608 MPa and a maximum total deformation of 2.5538 mm, giving a factor of safety of 16.3 against the 40 MPa yield strength of ABS. The first five natural frequencies (41.67 Hz to 69.73 Hz) fell outside the propeller excitation band, confirming resonance avoidance. Steady-state thermal analysis returned a peak surface temperature of 51.021 °C, well below the 110 °C softening point of ABS, while combined thermal-mechanical loading raised the equivalent stress to only 12.456 MPa. The frame prototype was fabricated using the Creality CR-6 SE 3D printer, producing an assembled mass of 1.05 kg, which is 21% of the 5 kg maximum take-off weight, with dimensional deviation held within ±0.2 mm. Physical validation by static load and by drop tests from 0.25 m and 0.5 m (impact velocities of 2.215 m/s and 3.132 m/s) produced no cracking, layer separation or permanent deformation, supporting the simulation findings. Overall, the research demonstrates the feasibility of using low-cost 3D printing and polymer-based materials to produce functional UAV structures, offering significant reductions in manufacturing cost while maintaining mechanical reliability and operational safety.

Keywords: *Drone frame, Precision agriculture, Finite Element Analysis (FEA), Computer-Aided Design (CAD), 3D printing, Quadcopter.*

1.0 Introduction

1.1 Background of the Study

Unmanned Aerial Vehicles (UAVs), or drones, have emerged as transformative tools in precision agriculture, effectively supplementing satellite-based systems by enabling high-resolution, on-demand field monitoring. Their low-altitude operational capability facilitates detailed data collection for tasks ranging from crop health assessment and soil variability analysis to targeted spraying and irrigation management [1]. Compared to traditional manual scouting, drone surveillance offers a faster, less labour-intensive, and more economical alternative. Advances in autonomous navigation have further enhanced this utility, enabling real-time field assessments with minimal human intervention, with drones surveying hectares of land in minutes while streaming data to base stations [2]. This proven effectiveness has catalyzed sustained research into optimizing UAV platforms for specialized agricultural needs.

A critical, yet often underexplored, component of this optimization is the physical airframe. The performance of an agricultural drone its flight endurance, stability, payload capacity, and resilience to field conditions is fundamentally constrained by the design of its frame [3]. The pursuit of a structure that is both lightweight for energy efficiency and robust enough to withstand operational stresses represents a core engineering challenge. The iterative process of building and testing physical or digital models allows designers to evaluate performance, identify flaws, and refine designs before final production, thereby reducing development time and increasing reliability [3].

In recent years, virtual prototyping using sophisticated simulation tools has become a powerful complement to physical models. Engineers can now subject digital drone frames to simulated environmental stresses such as wind loads, mechanical impacts, and varying payloads to predict real-world behavior without the cost and time of building multiple physical iterations. This approach can significantly reduce development expenses [4]. However, physical prototyping remains essential for final validation and performance verification. Thus, a synergistic approach combining virtual simulation with tangible manufacturing techniques like 3D printing represents a modern, efficient pathway for frame development. Despite these methodological advancements, a distinct research gap persists. While scholarly and industrial efforts have heavily concentrated on improving UAV sensor payloads, flight control algorithms, and general system integration, the dedicated structural design of lightweight frames optimized for agricultural deployment has received comparatively scant attention. Specifically, the gap addressed in this work is the absence of a single study that carries a mission-defined agricultural frame through sizing calculations, static, modal and thermal finite element analysis, and low-cost polymer 3D printing, and then validates the printsed frame experimentally. Existing studies stop at either the simulation stage [13], [23], [27] or the fabrication stage, so the link between predicted and measured structural behaviour of a printed agricultural UAV frame remains unverified.

Simulation engineering has been instrumental in accelerating UAV development by allowing researchers to evaluate and refine design parameters virtually before physical fabrication. Matsson [5] introduced ANSYS Fluent as a tool for analyzing fluid dynamics and aerodynamic behaviour in UAV designs. Through CFD simulations, designers can predict how air flows around the drone frame, optimize structural configurations, and reduce development cycles. These simulations are particularly useful in minimizing drag, enhancing lift, and identifying weak points in the design [6].

Simulation-driven design allows engineers to explore multiple configurations, test stress points, evaluate vibration modes, and assess aerodynamic performance in a virtual environment. Karlberg et al. [6] described simulation-driven design as a shift from intuition-based modelling to data-driven engineering that enables optimization before fabrication. It offers several advantages; Virtual prototyping significantly cuts material waste and the need for physical testing [7]. Design iterations are tested within hours rather than days or weeks [8]. Early-stage detection of structural weaknesses or dynamic instability allows modifications tailored to specific payloads or mission types in UAV applications.

UAV design requires various simulation modalities, including:

i. Static Structural Simulation: Evaluates deformation and stress under steady loads [9].
ii. Modal and Vibration Analysis: Identifies natural frequencies and vibration modes critical to flight stability [10].
iii. Thermal Simulation: Assesses component behaviour under heat dissipation from motors and batteries.
iv. Computational Fluid Dynamics (CFD): Used for analyzing aerodynamic behaviour, especially in propeller-rotor interaction and fuselage airflow [11].
v. Impact and Fatigue Simulations: Predict how long the drone frame can last under repeated load cycles [12].

SolidWorks and ANSYS dominate due to their wide availability and intuitive interfaces.

Several studies demonstrate how simulation was applied to optimize drone frames:

Harika [13] conducted a comparative material analysis using SolidWorks Simulation to determine the suitability of PLA vs. ABS in quadcopter frames. The study revealed stress concentration near motor hubs and arms when loaded, leading to frame reconfiguration that enhanced structural performance by 28%.

Veeraperumal [14] used ANSYS Workbench to assess the structural integrity of the rotary UAV empennage. Their hybrid rotor structure exhibited superior resistance to aeroelastic deformation under load.

Štoller & Dubec [11] applied CFD techniques in Ansys Fluent to evaluate the aerodynamic shape of protective structures, a method transferable to drone airframe optimization, especially when designing for minimal drag and maximum stability.

Such applications show that simulation not only validates concepts but guides weight minimization and structural enhancement, critical in drone designs where every gram affects flight time and stability.

The primary engineering challenges in developing such a frame include:

1. The Strength-to-Weight Dilemma: Lightweight materials often compromise durability, making frames vulnerable to damage from impacts, rough landings, and field hazards [15].
2. Flight Performance Trade-offs: While weight reduction improves battery life and flight time, it can introduce instability and vibration if structural integrity and aerodynamic balance are not meticulously engineered [2, 16].
3. Cost-Effectiveness for Scalability: High-performance materials like carbon fiber increase cost, presenting a barrier to adoption, particularly in resource-limited settings. Balancing affordability with structural integrity is crucial [17].

Received: 06/07/2026; Revised: 22/07/2026; Accepted: 30/07/2026; Published: 15/08/2026

4. Payload Integration: The frame must accommodate various sensors and equipment without compromising flight dynamics or stability, ensuring reliable data acquisition during extended missions [2].

To address this gap and these challenges, this study focuses exclusively on the design, analysis, and fabrication of a lightweight drone frame specifically intended for agricultural monitoring. The research is guided by the overarching aim to develop a structurally efficient frame that enhances flight stability and endurance without sacrificing robustness. This is achieved through an integration of finite element simulation and additive manufacturing, that is, the layer-by-layer building of a component directly from a digital model, which in this work is implemented as fused deposition modelling (FDM) of ABS filament.

Precision agriculture uses site-specific crop management to improve productivity and resource efficiency. Unmanned Aerial Vehicles (UAVs) play a major role in achieving these goals through several applications. Drones equipped with Red-Green-Blue (RGB) and multispectral cameras are used for aerial mapping and photogrammetry to create georeferenced maps and digital elevation models for land-use planning and drainage management [18]. They are also used for vegetation health monitoring through the Normalised Difference Vegetation Index (NDVI) and thermal imaging, which help detect plant stress, diseases, and irrigation problems [19].

Another important application is targeted spraying using Variable Rate Application (VRA), where fertilisers, herbicides, or pesticides are applied only to affected areas, thereby reducing waste and environmental impact. UAVs are also increasingly used for yield estimation and crop growth prediction through machine vision and artificial intelligence integrated with crop models. The present work is directed at one of these applications in particular, namely low-altitude crop health monitoring of cereal and vegetable plots. In this task, the drone flies at 50 m to 120 m above ground level carrying a multispectral camera and gimbal of 0.5 kg to 0.7 kg, and covers 5 ha to 20 ha per sortie in order to generate NDVI maps for early detection of nutrient deficiency, pest infestation and water stress [18], [19]. This mission, rather than heavy spraying or seed-broadcasting duty, defines the payload, endurance and structural requirements used throughout the design.

Despite their benefits, agricultural drones face several limitations. One major challenge is limited battery life, as most multi-rotor drones can only fly for 20–40 minutes per charge, especially when carrying additional sensors or spraying equipment. Payload capacity is another issue because increasing payload often reduces flight endurance. This creates a need for lightweight yet durable frame designs. These endurance and payload limitations are consistently reported in recent reviews of UAV deployment in precision agriculture [18], [19].

High costs of advanced drones, maintenance, and pilot training also limit adoption, particularly in low-income regions. Environmental conditions such as wind, rain, and extreme temperatures further affect drone performance, making structural protection and stability essential for reliable field operations. Similar constraints on cost, maintenance and environmental exposure have been documented for field operations in developing agricultural economies [21].

Structural stability is critical in agricultural UAV design. Lightweight frames improve manoeuvrability and flight duration but may reduce resistance to wind disturbances and mechanical stress. [20] reported that material selection and geometric configuration strongly influence UAV durability and flight stability. Agricultural drones often operate under harsh conditions involving wind, moisture, and repeated take-offs and landings, increasing the need for strong and resilient frames [21].

Common UAV frame materials include Carbon Fibre Reinforced Polymer (CFRP), PLA, ABS, and aluminium alloys. [13] found that carbon fibre performed better than PLA and ABS in vibration resistance, stress distribution, and durability, although PLA remains useful for low-cost prototypes.

A comparison of the candidate frame materials is therefore necessary before selection. Carbon Fibre Reinforced Polymer (CFRP) offers the highest specific stiffness and the best vibration damping, but it requires moulding tools, autoclave or vacuum-bagging facilities and skilled labour, which places it out of reach for low-budget prototyping and repair in the field. Aluminium alloys such as 6061-T6 are readily available and easily machined, but their density of about 2.70 g/cm³ is roughly 2.6 times that of ABS, and they require machining or welding rather than direct printing. Polylactic Acid (PLA) prints more easily than ABS and is stiffer, but it softens near 60 °C and is brittle on impact, which makes it unsuitable for a frame that must survive direct sunlight and repeated hard landings in the tropics [13], [24]. ABS was therefore selected for this work because it combines a low density of 1.02 g/cm³ and a tensile yield strength of 40 MPa with a glass transition temperature near 105 °C, good impact toughness, solvent bondability using acetone, and full compatibility with low-cost desktop FDM printers, so that a damaged arm can be reprinted and replaced on site at negligible cost [25], [26]. The quantitative comparison is presented in Table 1.

Dynamic loading from payloads and turbulence also affects UAV structures. [22] showed that payload attachment increases stress around drone arms and landing gear, while turbulence causes greater torsional and bending deformation. Frame geometry such as X-frame configurations improves weight distribution and thrust balance, making them suitable for precision agriculture [13].

Other research works on drone frame development further inform the present design. Singh et al. [23] carried out a structural analysis of a quadcopter frame and showed that stress concentrates at the arm-to-hub interface

Received: 06/07/2026; Revised: 22/07/2026; Accepted: 30/07/2026; Published: 15/08/2026

and at the motor mounts, which is the same critical region identified in this study. Patil et al. [27] performed transient and modal analysis of a UAV frame and established that the first bending mode of the arms governs the resonance margin, confirming the need for the modal study reported in Section 3.2. Stanislaus Arputharaj et al. [22] investigated an agricultural drone with and without payload devices and reported that payload attachment raises arm and landing-gear stress appreciably, which justifies the payload-inclusive loading adopted here. Harika et al. [13] compared PLA and ABS in an X-frame quadcopter and reported a 28% improvement in structural performance after reconfiguration of the arm geometry. What these works have in common is that they terminate at the simulation stage; none of them prints and physically tests the analysed frame, which is the contribution made by the present study.

Hence, the objectives of this study are to: (i) develop a detailed 3D model of a lightweight multi-rotor UAV frame optimised for agricultural monitoring; (ii) carry out static, modal, steady-state thermal and thermal-stress finite element analyses of the frame under operational loads; (iii) fabricate the optimised design by FDM 3D printing; and (iv) validate the printed prototype experimentally by static load and drop testing. The methodology in Section 2 is arranged to follow these four objectives in order.

2.0 Materials and Methods

This section describes the software and hardware resources used, the design considerations and sizing calculations, the finite element analyses performed, and the 3D printing procedure adopted. The sub-sections follow the order of the objectives stated in Section 1.

2.1 Materials and Equipment

The resources used in this work comprise the modelling and analysis software, the 3D printing hardware, and the polymer feedstock, each described below.

2.1.1 Software Tools

The frame was modelled in SolidWorks 2023. The body frame was divided into four separately modelled components, namely the central hub, the four arms, the landing rack and the motor mounts. Each component was modelled as an individual part file, fully dimensioned, and the parts were subsequently brought together in an assembly file using mate constraints. The individual part drawings, in 2D and 3D with dimensions, are presented in Appendix A. The size of the four arms are equal.

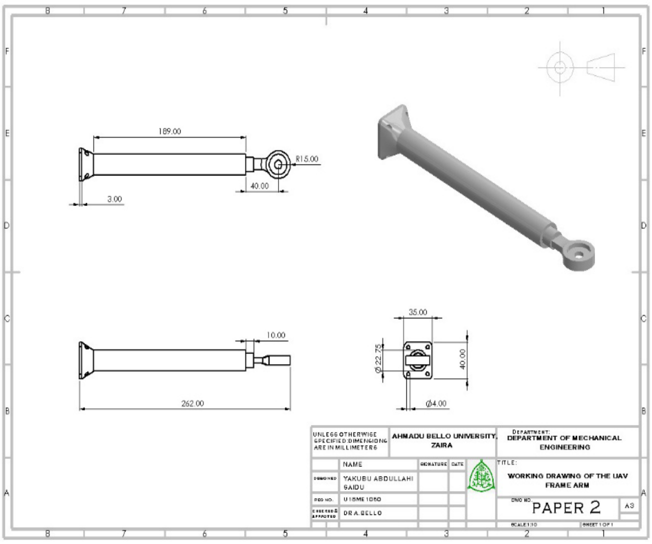

Figure 1: Working drawing of the UAV frame arm

Received: 06/07/2026; Revised: 22/07/2026; Accepted: 30/07/2026; Published: 15/08/2026

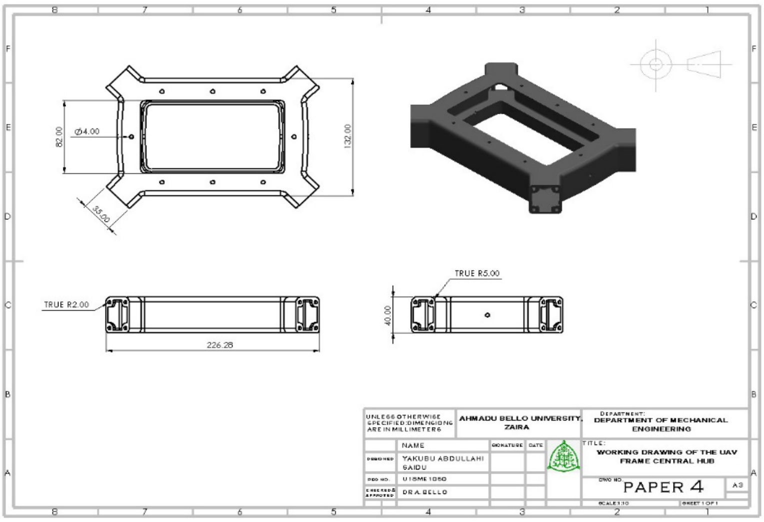

Figure 2: Working drawing of the UAV frame central hub

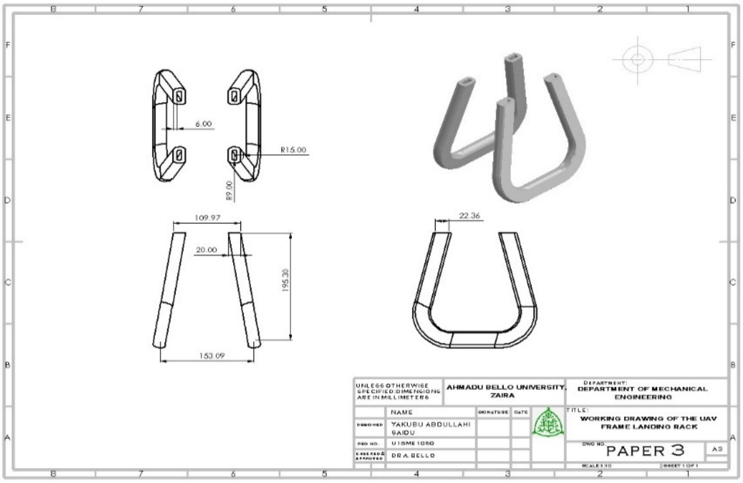

Figure 3: Dimensioned 2D drawings of the frame components

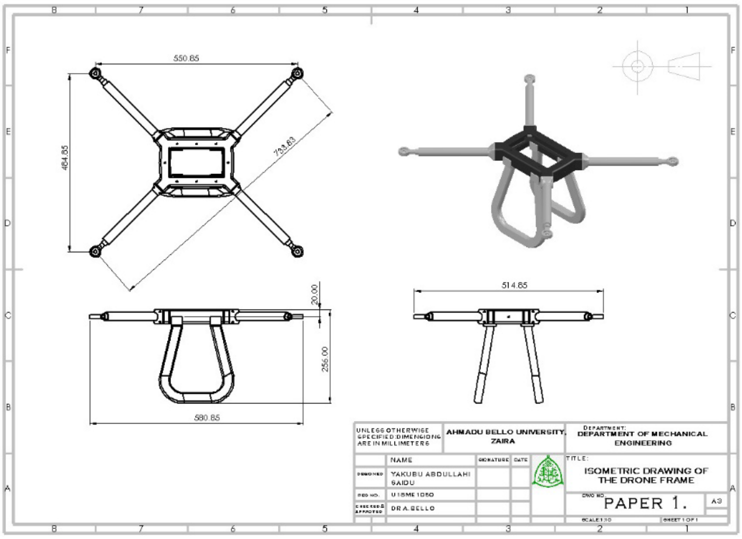

Plate 1a: Isometric view of the drone frame

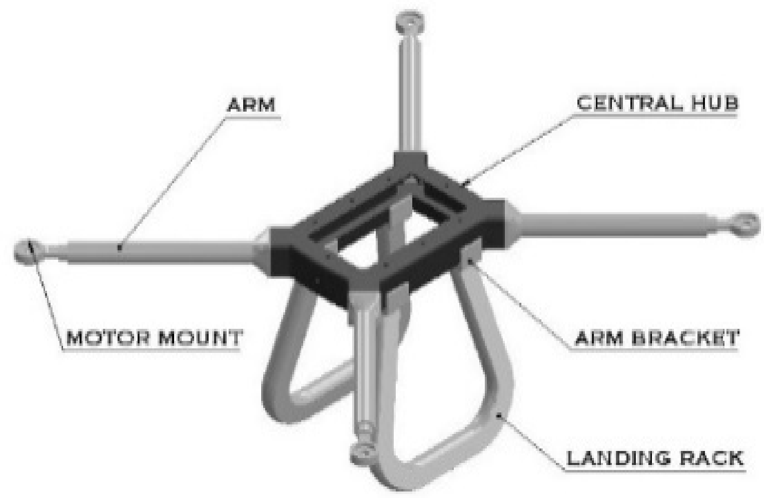

Plate 1: Assembled CAD model of the proposed drone frame

The drone frame, referred to hereafter as the quadcopter frame since the design is a four-rotor configuration, was analyzed to evaluate its feasibility, rigidity, and compatibility using ANSYS Mechanical 2024 [23]. Rigidity of the quadcopter body frame was analyzed considering the equality between the vertical thrust produced by each motor and the weight of the quadcopter during flight time. In addition to mechanical loading, thermal effects such as exposure to solar radiation and convection were also considered to ensure that temperature variations would not induce material softening or deformation in the ABS frame.

2.1.2 Hardware Tools (3D printer)

The Creality CR-6 SE 3D printer was employed for the fabrication of the UAV frame prototype. The printer features a build volume of 235 × 235 × 250 mm, making it suitable for medium-scale component printing, such as the drone's arms and central hub. The printer uses Fused Deposition Modelling (FDM) technology and supports a variety of thermoplastics, including PLA, PETG, and ABS, when operated in a temperature-controlled environment or enclosed setup. A photograph of the printer used is presented in Plate 6.

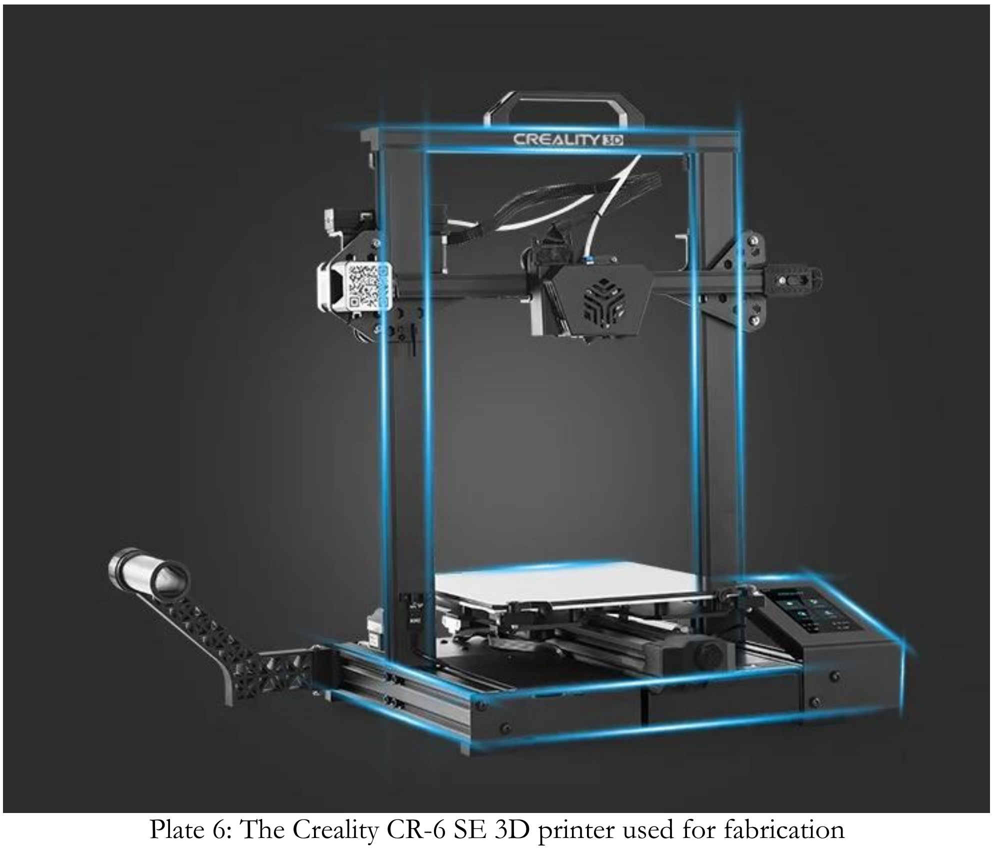

Plate 6: The Creality CR-6 SE 3D printer used for fabrication

Received: 06/07/2026; Revised: 22/07/2026; Accepted: 30/07/2026; Published: 15/08/2026

2.1.3 Material Selection (ABS filament)

Acrylonitrile Butadiene Styrene (ABS) was selected as the primary printing material due to its favourable balance of mechanical strength, impact resistance, and printability. ABS has a density of approximately 1.02 g/cm³ and a tensile yield strength of 40 MPa [24, 25 & 26], providing sufficient structural performance for lightweight UAV frames when printed with proper layer orientation.

Table 1: Comparison of candidate materials for UAV frame development [13], [24], [25], [26]

Material	Density (g/cm³)	Tensile yield strength (MPa)	Service temp. limit (°C)	Relative cost	Suitability for this work
CFRP	1.55 - 1.60	600 – 900	> 150	Very high	Best stiffness but needs moulds and skilled labour
Aluminium 6061-T6	2.70	276	> 200	Moderate	Heavy; requires machining, not printable
PLA	1.24	50 – 60	≈ 60	Low	Brittle; softens under tropical sun
ABS	1.02	40	≈ 105	Low	Selected: low density, tough, printable, solvent bondable

2.2 Design Considerations

The frame was designed against the standard engineering design considerations applicable to a structural airframe, namely functional requirement, strength and stiffness, weight, material availability and cost, manufacturability, and safety. Each of these is addressed in turn below, and the resulting values are carried forward into the sizing calculations of Section 2.3.

Design Purpose and Payload: The frame was designed for field crop monitoring, capable of carrying lightweight sensors such as a multispectral camera (0.5-0.7 kg) with a gimbal, alongside necessary electronics and batteries.

Operational Parameters

- Field Coverage: 5–20 hectares per mission.
- Flight Altitude: 50–120 m AGL (compliant with VLOS regulations and suitable for 3–10 cm/pixel imagery).
- Flight Speed: A moderate 5–10 m/s for stable imaging.
- Configuration: Multirotor VTOL for operation without runways.
- Weight Limit: Maximum Take-off Weight (MTOW) kept under 5 kg to align with small UAS regulations.

These operational values were not assumed arbitrarily. The field coverage of 5 ha to 20 ha corresponds to the typical smallholder plot size served in a single sortie and follows the coverage reported for multispectral survey missions [18]. The altitude band of 50 m to 120 m is set by the Nigeria Civil Aviation Authority visual-line-of-sight ceiling of 120 m and by the ground sample distance of 3 cm to 10 cm per pixel required for NDVI interpretation at the sensor focal length used [19]. The speed of 5 m/s to 10 m/s is the range over which motion blur remains below one pixel for the camera exposure time. The 5 kg maximum take-off weight is the upper bound of the small unmanned aircraft category, and the thrust-to-weight ratio of 2.0 is the accepted minimum for adequate control authority of a multirotor in gusty conditions [20]. The payload mass of 0.7 kg, the electronics mass of 0.8 kg and the battery mass of 1.2 kg were taken from the datasheet masses of the components selected for the build.

The heat conduction problem is solved by the following boundary conditions:

i. A steady-state heat flux equivalent to solar exposure (1000 W/m²) was applied to the surfaces of the frame
ii. Convective boundary condition with ambient air temperature of 40 °C
iii. Heat transfer coefficient h = 20 W/m² K was also defined.

2.3 Design Calculations

This section presents only the design calculations, that is, the propulsion sizing, the arm bending analysis, the factor-of-safety check and the frame mass estimate. The input data used were established in Section 2.2.

The DJI Agras T100 Agricultural drone was taken as a reference point in choosing the appropriate geometry to ensure an adequate design. The thrust-to-weight ratio of 2.0 was chosen to provide sufficient control reserves during flight manoeuvres and strong winds.

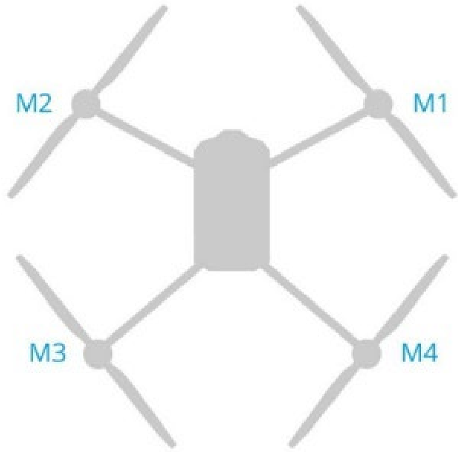

Figure 1: Schematic diagram of the quadcopter frame showing the arm length Larm

The design inputs carried forward from Section 2.2 are a payload mass of 0.7 kg (camera plus gimbal), an electronics and control system mass of 0.8 kg, and a battery mass of 1.2 kg.

The arm length Larm was set at 262 mm from the propeller clearance requirement of the 14 in propeller selected, so that adjacent propeller discs do not overlap in the X-configuration.

Propeller: 14 × 4 (14 in diameter, 4 in pitch; plastic/carbon composite). The low pitch was selected to favour static thrust and hover efficiency rather than forward speed, which suits the low-speed survey mission defined in Section 2.2.

$$\mathrm{MTOW} = \mathrm{m_{payload}} + \mathrm{m_{frame\ estimate}} + \mathrm{m_{battery}} + \mathrm{m_{electronics}} + \mathrm{contigency\ (\%)}$$ [20]

The Maximum Take-Off Weight MTOW estimate = 5 Kg The maximum take-off weight relation and the thrust-per-motor relation used here are the standard multirotor sizing expressions given in [20], and the bending stress relation σ = Mc/I is the elementary beam bending formula [28], [29].

For a quadcopter configuration (n = 4)

Table 2: Design calculations

Initial Data	**Calculations**	**Result/Remark**
$m_{payload} = 0.7$ Kg $m_{electronics} = 0.8$ Kg $m_{battery} = 1.2$ Kg	$MTOW = m_{payload} + m_{frame\ estimate} + m_{battery} + m_{electronics} + contigency\ (\%)$	m payload + m electronics + m battery = 2.70 kg; plus m frame = 0.883 kg gives 3.58 kg; plus propulsion set, wiring and fasteners with contingency gives MTOW = 5.00 kg MTOW = 5 Kg
T/W = 2.0 n = 4	$Thrust_{per\ motor} = \dfrac{MTOW\ \times g\ \times \frac{T}{W}}{n}$	$T_{per\ motor} = 24.5$ N The thrust per motor is chosen to be 25 N
$D_{out} = 22.75$ mm $D_{in} = 16.75$ mm $L_{arm} = 262$ mm $T_{per\ motor} = 25$ N	$\sigma = \dfrac{M.c}{I}$ $M = T_{per\ motor} \times L_{arm}$ $I = \dfrac{\pi}{64}({D^4}_{out} - {D^4}_{in})$ $c = \dfrac{D_{out}}{2}$	I = 9285.16 mm^4 c = 11.375 mm Moment = 6.55 KN.mm Bending stress σ = 8.02 MPa
F.o.S = 1.5 $\sigma_{eff} = 40$ MPa	$FoS = \dfrac{\sigma_{eff}}{\sigma_{allow}}$	σ allow = σ eff / FoS = 40 / 1.5 = 26.7 MPa $\sigma_{eff} = 40$ MPa $\sigma_{bending} \leq \sigma_{allow}$ 8.02 MPa ≤ 26.7 MPa (safe)

Received: 06/07/2026; Revised: 22/07/2026; Accepted: 30/07/2026; Published: 15/08/2026

Initial Data	Calculations	Result/Remark
Volume of the Frame = 0.000866 m^3 (value gotten from the mass properties of the design)	$\rho_{ABS} = \frac{mass\ of\ the\ frame}{volume\ of\ the\ frame}$	The mass of the Frame = 0.883 Kg

2.4 Simulation and Analysis

Four analyses were carried out on the frame, namely a static structural analysis, a modal analysis, a steady-state thermal analysis coupled to a thermal-stress analysis, and a drop test. The overall sequence is summarized in the methodology flowchart of Figure 2.

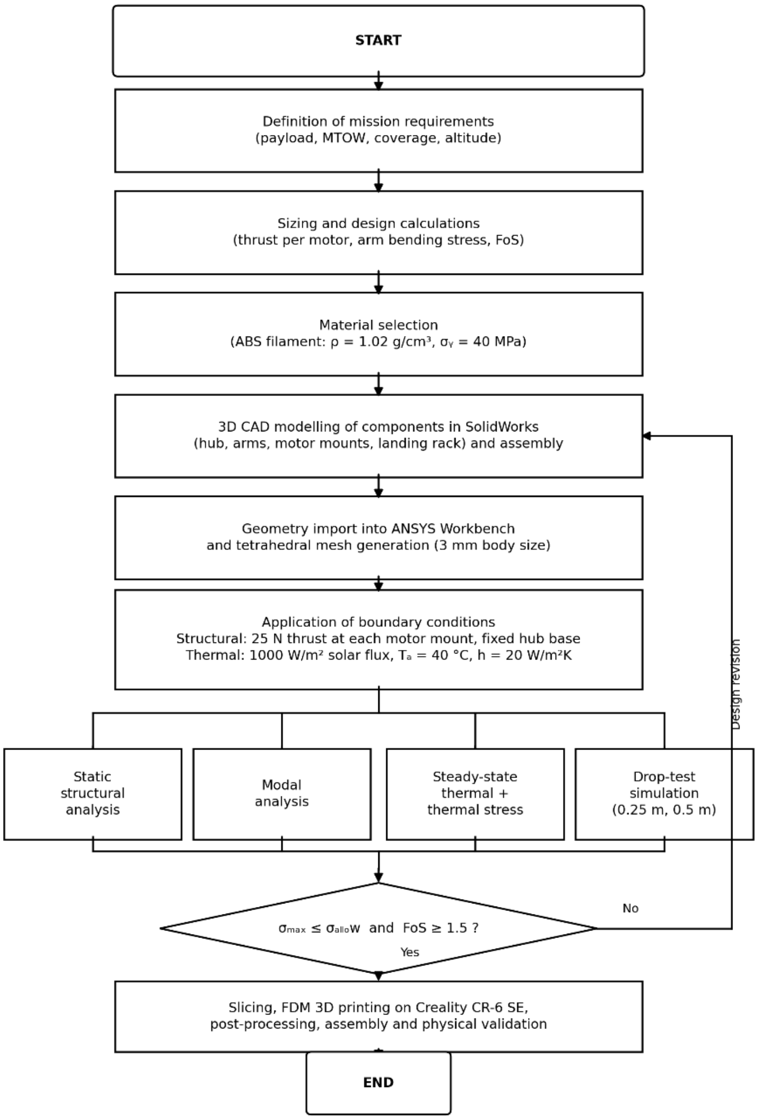

Figure 2: Flowchart of the design, simulation and fabrication methodology

2.4.1 Finite Element Analysis (FEA)

FEA evaluated the structural and thermal performance of the SolidWorks assembly model of the frame, imported into ANSYS Workbench as a Parasolid solid body, by discretizing it into tetrahedral elements, applying the thrust and thermal boundary conditions of Section 2.4.2, and solving the governing equilibrium equation $[K]\{u\} = \{F\}$ for the structural case and the steady-state heat conduction equation $\nabla \cdot (k\nabla T) + q = 0$ for the thermal case [28], [29]. The analysis showed how ABS, as a lightweight polymer, responds to the operational stresses and heat loads; the quantitative outcomes are reported in Section 3.

2.4.2 Structural Load Application

The drone frame was subjected to realistic loads derived from thrust and payload conditions [27]. Each motor generated an estimated upward thrust of up to 25 N, sufficient to counteract the total weight of the UAV. Assuming equal thrust distribution across the four arms, the applied load per arm corresponded to one-fourth of the Maximum Take-Off Weight (MTOW). Thermal loads were also considered for the steady-state thermal analysis. The loading method adopted is that of Singh et al. [23], in which the motor thrust is applied as a distributed force on each motor mount face while the central hub base is fully fixed, and it was applied here without modification.

Mesh generation was conducted using a tetrahedral element type for complex geometry capture. The mesh density was refined in high-stress regions, such as arm joints and the central hub, to improve accuracy while maintaining computational efficiency. An element body size of 3 mm was picked and refined through a mesh convergence study to balance precision and runtime.

2.4.3 Static Structural Analysis

The Static Structural Analysis was used to determine the Equivalent (von-Mises) stress, Total deformation, and strain distribution under steady loads. This analysis identified how the frame would behave under maximum take-off and landing conditions, simulating a payload scenario [27].

The thrust generated by the motor propeller set is applied at the four corners and the base is made to be fixed. Results were evaluated against the yield strength of ABS to ensure that the induced stresses remained below the material's elastic limit. The Factor of Safety (FoS) was calculated as the ratio of yield strength to maximum equivalent (von Mises) stress. A factor of safety of greater than or equal to 1.5 was targeted to ensure durability and resilience during prolonged operation.

2.4.4 Modal Analysis

Modal analysis is the fundamental of dynamic analysis, and was performed to determine the natural frequencies and mode shapes of the UAV frame [27].

The objective was to ensure that the frame's natural frequency remained well above the motor and propeller excitation frequencies. This prevents resonance-induced fatigue and instability, thus enhancing flight performance and component lifespan.

2.4.5 Steady-State Thermal Analysis

A steady-state thermal analysis calculates the effects of steady thermal loads on a system or component to determine temperature, heat flux, and directional heat flux as the solution. This is done when the temperature distribution is unknown but we want to calculate the temperature field [28, 29].

The thermal boundary values below follow from the environmental design considerations of Section 2.2, namely peak tropical solar irradiance and peak ambient shade temperature at the intended operating location.

A thermal stress problem is later simulated to see how the design will deform under both thermal and structural loads. This is done by connecting the thermal and structural systems in the Workbench project schematics, which automatically transfers the non-uniform temperature field calculated in thermal analysis as an input condition for the structural analysis. The Equivalent (von-Mises) stress, Total deformation, and strain distribution are recalculated using the previous boundary conditions of the static structural analysis.

2.4.6 Drop Test

The drop test was conducted to assess the frame's ability to withstand low-altitude impact forces that occur during hard or emergency landings [30].

The 3D-printed frame (ABS) was released from a controlled height of 0.25 m and 0.5 m, corresponding to impact velocities of approximately 2.215 m/s and 3.132 m/s respectively. These velocities were obtained from the free-fall relation $v = \sqrt{2gh}$ with $g = 9.81\ m/s^2$, giving $v = \sqrt{2 \times 9.81 \times 0.25} = 2.215\ m/s$ and $v = \sqrt{2 \times 9.81 \times 0.5} = 3.132\ m/s$. The two heights represent a normal hard landing and an emergency drop from hover taxi height respectively.

2.5 3D Printing Procedure

The prototype of the lightweight drone frame used fused deposition modelling (FDM) technology. The process involved printer setup, slicing, printing, and post-processing operations. The printing procedure adopted is the standard FDM workflow for ABS described by An et al. [25] and by Raise3D [24], namely printer calibration, slicing, printing in an enclosed chamber, and post-processing.

2.5.1 Printer Settings and Calibration

The Creality CR-6 SE was calibrated using bed levelling and optimized settings, including a nozzle temperature of 235 °C and a bed temperature of 110 °C for ABS adhesion. The extrusion flow and retraction were also fine-tuned to ensure uniform printing and prevent defects. The full parameter set is given in Table 3.

2.5.2 Slicing and G-code Generation

The designed drone frame model from SOLIDWORKS was exported in STL format and processed using Creality Slicer (based on Cura Engine) slicing software. The slicing process translated the 3D model into machine-readable G-code, defining toolpath movements, extrusion rates, and layer sequences.

During slicing, the model was oriented to minimize overhangs and reduce the need for support material, thereby conserving filament and maintaining surface quality. The frame components were divided into sections for separate printing and later assembly. The G-code was then transferred to the printer via USB for execution.

2.5.3 Printing Parameters

To ensure strong interlayer bonding and minimal print defects, the following parameters were adopted.

Table 3: 3D printer parameter settings (source: Creality product documentation)

S/N	Parameter	Value/Setting
1.	Layer Height	0.2 mm
2.	Infill Density	60%
3.	Infill Pattern	Gyroid
4.	Print Speed	80 mm/s
5.	Nozzle Temperature	235°C
6.	Bed Temperature	110°C
7.	Cooling Fan	20% Speed

Parts were printed separately to maintain precision and allow ease of post-processing.

2.5.4 Post-processing Steps

After printing, the components were allowed to cool gradually within the printer enclosure to avoid thermal shock. Supports were then carefully removed using a deburring tool and fine-grit sandpaper to smooth the surface. The printed parts were joined using ABS slurry (a mixture of ABS and acetone) to ensure chemical bonding between interfaces. The assembled frame was then left to cure for 12 hours at room temperature.

Dimensional accuracy was verified using digital callipers, and the final assembly was inspected for symmetry, alignment, and overall surface quality.

3.0 Results and Discussion

The results of the four analyses and of the physical tests are presented in this section. In each sub-section, the quantitative results are first tabulated, after which the contour plots are shown, and the findings are discussed and compared with those of other researchers.

3.1 Static Structural Analysis

The static structural analysis evaluated the frame deformation, stress, and strain distribution under steady thrust and payload. The results are summarised in Table 4, and the corresponding contours are shown in Plate 2a-c.

Table 4: Summary of static structural analysis results

Parameter	**Value**	**Location of maximum**	**Remark**
Maximum equivalent (von Mises) stress	2.4608 MPa	Motor mount to arm junction	Below 40 MPa yield strength of ABS
Maximum total deformation	2.5538 mm	Arm tip	Within the 3 mm success criterion
Maximum equivalent elastic strain	0.0012369	Motor mount to arm junction	Wholly elastic; no yielding predicted
Reaction force at supports (Y)	24.05 N	Hub base	Balances applied thrust
Factor of safety (40 MPa / 2.4608 MPa)	16.3	-	Exceeds the target of 1.5

The maximum von Mises stress was 2.4608 MPa, the maximum total deformation 2.5538 mm and the maximum equivalent elastic strain 0.0012369, with the peak stress located at the motor mount-to-arm junction. The maximum stress remained below the ABS yield strength of 40 MPa, giving a factor of safety of 16.3 and confirming structural integrity. The maximum deformation of 2.5538 mm lies within the 3 mm limit set as the success criterion. The strain remained elastic, no yield was predicted, and the peak strain coincided with the high-stress region, indicating an elastic deformation response under the applied loads. The reaction force at the support points was 24.05 N in the Y direction, which balances the applied thrust and confirms equilibrium of the model.

Received: 06/07/2026; Revised: 22/07/2026; Accepted: 30/07/2026; Published: 15/08/2026

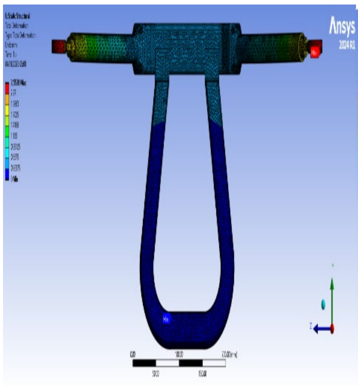

Plate 2a: Total deformation

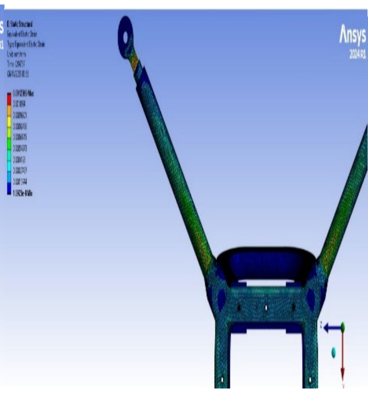

Plate 2b: Equivalent stress contour

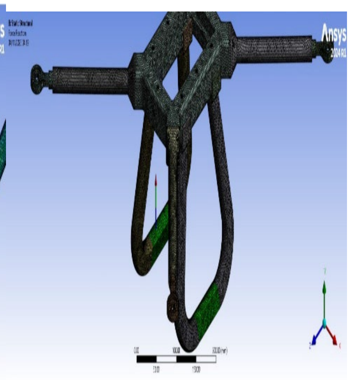

Plate 2c: Force reaction

These findings validated the load-bearing capability of the frame during hover and take-off. No plastic strain accumulation was predicted under the static load case, indicating elastic behaviour and no immediate yielding. The location of the peak stress agrees with Singh et al. [23], who also reported maximum stress at the arm-to-hub and motor-mount interfaces of a quadcopter frame, and with Harika et al. [13], who identified stress concentration near motor hubs and arms in an X-frame quadcopter. The present factor of safety of 16.3 is substantially higher than the values of about 2 to 4 typically reported for CFRP and aluminium frames [23], which is attributable to the conservative 3 mm arm wall thickness adopted here and indicates scope for further mass reduction in subsequent design iterations.

3.2 Modal Analysis

The modal results are summarised in Table 5 and the corresponding mode shapes are shown in Plate 3a-e. Five primary mode shapes were analysed, representing the total deformations experienced at the corresponding frequencies. The first mode involved vertical bending of the arms, while higher modes represented torsional movements about the hub and landing rack.

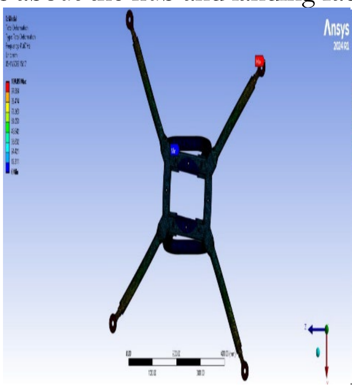

Plate 3a: First mode

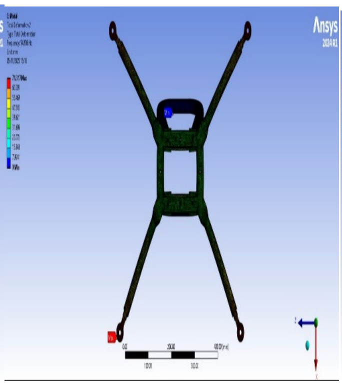

Plate 3b: Second mode

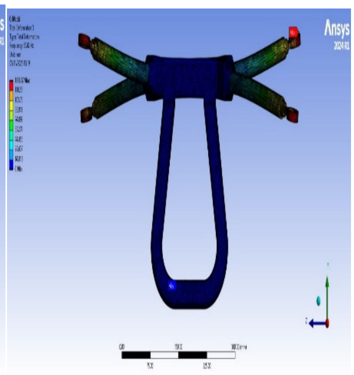

Plate 3c: Third mode

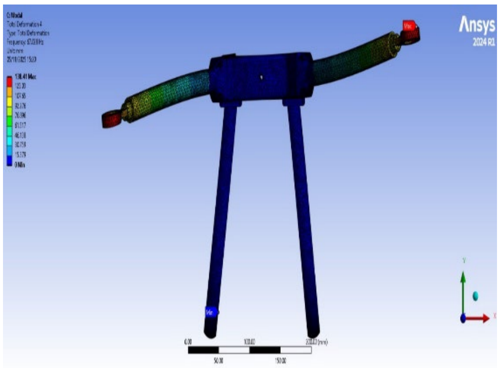

Plate 3d: Fourth mode

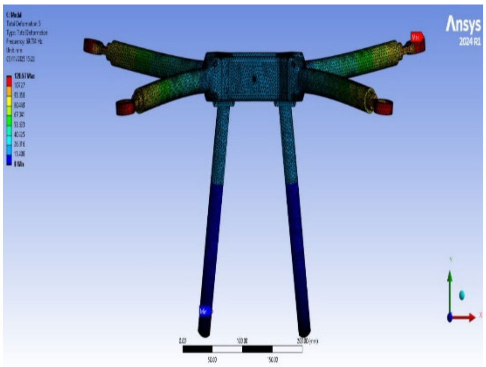

Plate 3e: Fifth mode

Table 5: Natural frequencies and mode shapes from the modal analysis

Mode	Natural frequency (Hz)	Dominant mode shape
1	41.670	Vertical bending of the arms
2	54.936	Vertical bending of the arms, out of phase

Mode	Natural frequency (Hz)	Dominant mode shape
3	59.020	Torsion about the central hub
4	67.028	Combined bending and torsion of the arms
5	69.734	Torsion of the landing rack

The first five natural frequencies were 41.670 Hz, 54.936 Hz, 59.020 Hz, 67.028 Hz and 69.734 Hz. For the 14 in propellers operating at a hover speed of about 4800 rpm, the blade passing excitation frequency is approximately 80 Hz, so the fundamental frequency of 41.670 Hz is separated from the excitation by a margin of more than 45%, satisfying the resonance avoidance criterion [10], [27]. The dominant modes corresponded to bending of the arms and twisting of the hub. The rigidity and geometric symmetry of the frame therefore keep vibration within safe operational levels. Patil et al. [27] reported a comparable fundamental frequency band of 35 Hz to 50 Hz for a UAV frame of similar span, which supports the present result.

3.3 Steady-State Thermal Analysis

Table 6: Summary of steady-state thermal analysis results

Parameter	Value	Remark
Minimum surface temperature	32.982 °C	Shaded underside of hub
Maximum surface temperature	51.021 °C	Well below the 110 °C softening point of ABS
Total heat flux	0.00878 W/mm²	Peak at arm-to-hub junction
Directional heat flux, X axis	0.001489 W/mm²	-
Directional heat flux, Y axis	0.004147 W/mm²	Dominant direction
Directional heat flux, Z axis	0.002590 W/mm²	-

The steady-state thermal results are summarised in Table 6 and the corresponding contours are shown in Plate 4a-e. A surface temperature range of 32.982 °C to 51.021 °C was recorded, with a total heat flux of 0.00878 W/mm² and directional heat fluxes of 0.001489 W/mm², 0.004147 W/mm² and 0.002590 W/mm² in the X, Y and Z directions respectively.

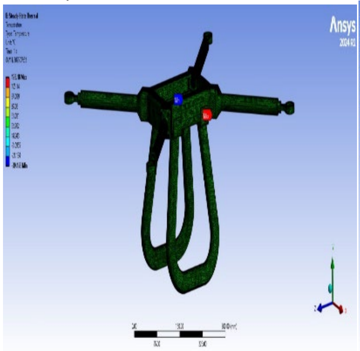

Plate 4a: Temperature contour

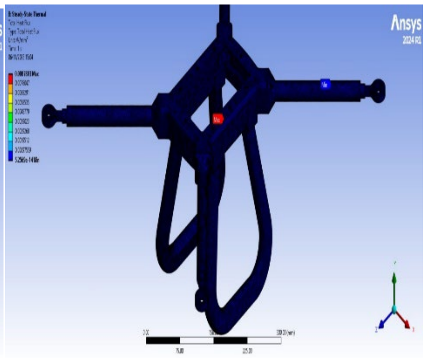

Plate 4b: Total heat flux

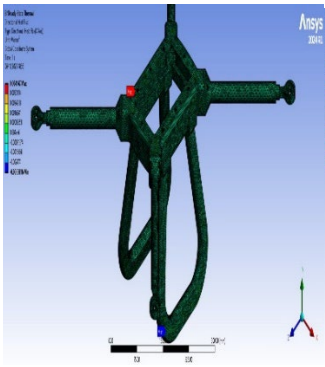

Plate 4c: Heat flux, X direction

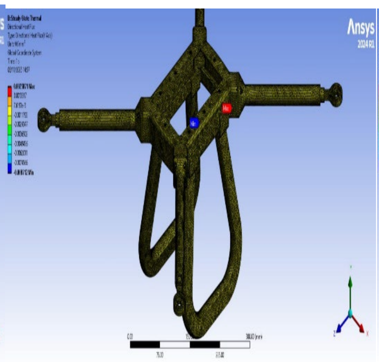

Plate 4d: Heat flux, Y direction

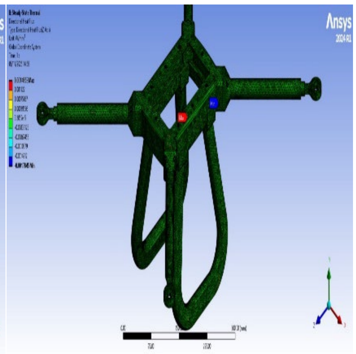

Plate 4e: Heat flux, Z direction

The results showed uniform temperature distribution along the frame, with uniform heat build-up. The highest temperature did not exceed ABS's softening point (110 °C), confirming thermal stability under solar exposure. The frame demonstrated effective heat dissipation across its surface area, with no indication of localized melting or excessive thermal gradients that could lead to material fatigue. The peak temperature of 51.021 °C leaves a margin of 54 °C below the 105 °C glass transition temperature of ABS, which is consistent with the thermal behaviour reported for printed ABS components by Park and Lee [26].

3.4 Thermal Stress Analysis

The thermal stress results are summarised in Table 7 and the contours are shown in Plate 5a-b.

An equivalent von Mises stress of 12.456 MPa and an equivalent total deformation of 2.5538 mm were recorded under combined thermal and mechanical loading.

Table 7: Comparison of static and combined thermal-mechanical stress results

Parameter	Static load only	Combined thermal and mechanical load	Remark
Maximum equivalent (von Mises) stress	2.4608 MPa	12.456 MPa	Still below the 40 MPa yield strength; FoS = 3.2
Maximum total deformation	2.5538 mm	2.5538 mm	Thermal expansion adds no measurable deflection

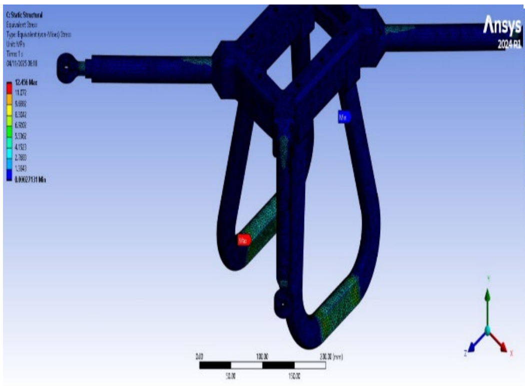

Plate 5a: Combined thermal stress

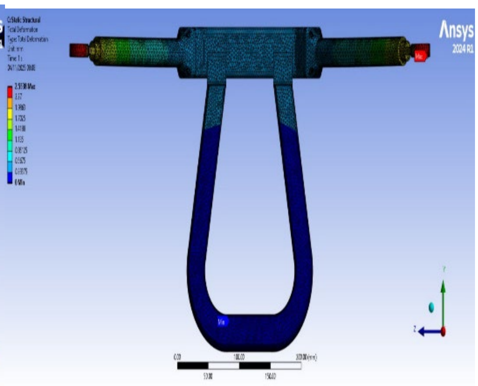

Plate 5b: Equivalent total deformation

The simulation revealed that the combined stress remained within the safe range of the material. Minor thermal expansion was observed at exposed arms, but it did not affect dimensional stability or flight balance. The thermal stress contours indicated that heat-induced deformation was negligible compared to mechanical loading effects. Thus, ABS material remained structurally reliable for extended outdoor operation. The five-fold increase in equivalent stress from 2.4608 MPa to 12.456 MPa on introduction of the thermal field shows that thermal loading, though not critical, is not negligible and should be retained in the analysis of polymer airframes. This agrees with Stanislaus Arputharaj et al. [22], who reported that environmental loading materially alters the stress distribution in agricultural drone structures.

3.5 Drop Test

Table 8: Results of the physical drop test

Drop height (m)	Impact velocity (m/s)	Observed damage	Permanent deformation	Outcome
0.25	2.215	None	None measurable	Pass
0.50	3.132	No cracking or layer separation	None measurable	Pass

The results of the physical drop test were recorded immediately after each impact to evaluate the frame's response to sudden loading conditions. For each test height (0.25 m and 0.5 m), the observed deformation was minimal, with no major cracks or failures detected in the arm joints, the central hub, or the landing rack region. No layer separation or surface chipping was observed.

The impact resilience of the frame indicated that the structure could safely absorb minor landing shocks or ground impacts without loss of functionality. Overall, the drop test evaluated that the 3D-printed ABS frame possessed sufficient impact resistance for use in small agricultural UAV applications. The findings confirmed the design's ability to withstand low-velocity impacts that may occur during take-off, landing, or unexpected ground contact. The absence of layer separation is notable because interlayer adhesion is the usual failure mode of FDM parts under impact; the result indicates that the 235 °C nozzle temperature and enclosed chamber produced adequate interlayer bonding, as reported by An *et al.* [25].

3.6 3D Printing Outcome

Table 9: Summary of the 3D printing outcome

Parameter	Value
Printer	Creality CR-6 SE (FDM)
Filament	ABS, 1.75 mm diameter
Number of printed components	5 (motor mounts, arms, arm brackets, central hub, landing rack)
Total print time	≈ 26 h
Filament consumed	0.9 kg
Final assembled frame mass	1.05 kg
Frame mass as fraction of 5 kg MTOW	21%
Dimensional deviation (digital callipers)	within ±0.2 mm
Visible warping or cracking	None observed

The drone frame was successfully fabricated using the Creality CR-6 SE 3D printer, following the finalised CAD model and slicing parameters. The printing process was completed in five stages: motor mounts, arms, arm brackets, central hub, and landing rack, with each part printed separately. The parts were later assembled using threaded inserts and epoxy bonding at the joints. The individual printed components are shown in Plate 7.

Each component was printed using ABS filament (1.75 mm diameter) with a layer height of 0.2 mm, an infill density of 60% and a nozzle temperature of 235 °C, as specified in Table 3. The total print duration for all components was approximately 26 hours, including short cooling intervals between prints. The overall material consumption was estimated at 0.9 kg.

Post-processing involved light sanding and acetone vapour smoothing to remove surface irregularities and improve inter-layer bonding. The final assembled frame weighed 1.05 kg, which was within the design specification and well below the 30% threshold of the estimated Maximum Take-Off Weight (MTOW).

No visible warping or cracking was observed, confirming that the controlled print temperature and partial enclosure were effective in stabilizing the ABS material. The overall print quality demonstrated that the Creality CR-6 SE was capable of producing structurally reliable UAV components at a low cost.

Received: 06/07/2026; Revised: 22/07/2026; Accepted: 30/07/2026; Published: 15/08/2026

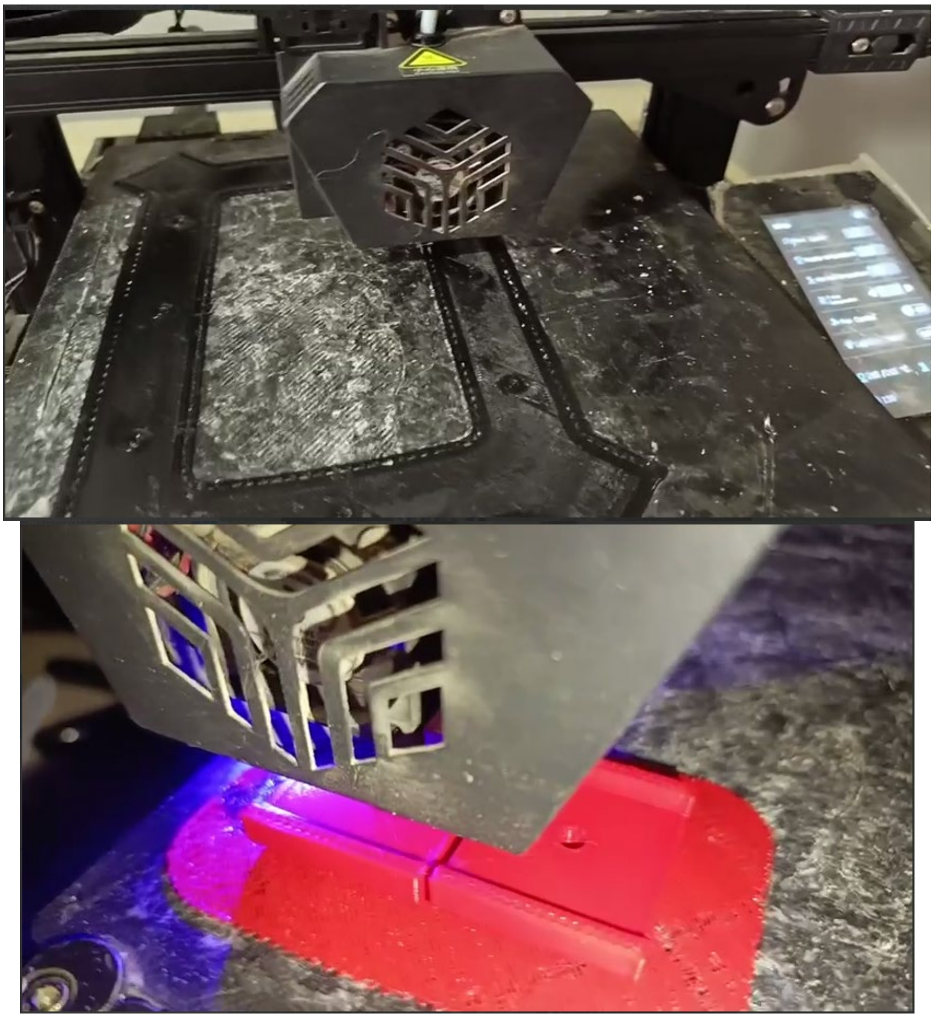

Plate 7: The printed components of the drone frame before assembly

4.0 Conclusion

The project successfully designed, simulated, fabricated and validated a lightweight 3D-printed drone frame for agricultural monitoring. The major findings are as follows. Under a thrust load of 25 N per motor arm, the frame developed a maximum equivalent stress of 2.4608 MPa and a maximum total deformation of 2.5538 mm, giving a factor of safety of 16.3 against the 40 MPa yield strength of ABS. The first five natural frequencies lie between 41.670 Hz and 69.734 Hz, more than 45% below the 80 Hz blade-passing excitation frequency, thereby avoiding resonance. Under a solar heat flux of 1000 W/m² at an ambient temperature of 40 °C, the peak surface temperature reached 51.021 °C, which is 54 °C below the glass transition temperature of ABS, and combined thermal-mechanical loading raised the equivalent stress only to 12.456 MPa, still a factor of 3.2 below yield. The frame was printed in five components in approximately 26 hours using 0.9 kg of filament, and the assembled frame weighed 1.05 kg, that is 21% of the 5 kg maximum take-off weight, with dimensional deviation within ±0.2 mm. Drop tests from 0.25 m and 0.5 m produced no cracking, layer separation or permanent deformation. The frame is therefore established as a viable, low-cost option for agricultural UAVs, and the work provides a practical base for future system integration.

It was, however, recommended that integrating a complete drone with sensors, flight controllers, and propulsion systems for in-flight testing and airworthiness assessment could enhance its performance. Also, the use of composite materials such as carbon-fibre-reinforced polymers to enhance stiffness and reduce vibrations while keeping weight low.

Acknowledgement

The authors acknowledge the technical support of the staff of the Department of Mechanical Engineering, Ahmadu Bello University, Zaria, for access to the 3D printing and metrology facilities used in this work, and the assistance of NAMES during the fabrication and testing stages.

Received: 06/07/2026; Revised: 22/07/2026; Accepted: 30/07/2026; Published: 15/08/2026

References

[1] C. Nakalembe, I. Becker-Reshef, R. Bonifacio, G. Hu, M. L. Humber, C. J. Justice, J. Keniston, K. Mwangi, F. Rembold, S. Shukla, F. Urbano, A. K. Whitcraft, Y. Li, M. Zappacosta, I. Jarvis, and A. Sanchez, "A review of satellite-based global agricultural monitoring systems available for Africa," *Global Food Security*, vol. 29, art. 100543, 2021.

[2] S. Raj, L. Chen and M. Ortega, "The efficacy of iterative prototyping in distributed design environments: a longitudinal study," International Journal of Design Studies, vol. 74, pp. 101-118, 2021.

[3] J. Wenngren and A. Rizk, The Prototype Imperative: Iterative Models and Systemic Reliability in Digital-Age Design. Cham, Switzerland: Springer, 2024.

[4] K. Crawford, The Atlas of AI: Power, Politics, and the Planetary Costs of Artificial Intelligence, 2nd ed. New Haven, CT, USA: Yale Univ. Press, 2023.

[5] J. Matsson, An Introduction to SolidWorks Flow Simulation 2023. Mission, KS, USA: SDC Publications, 2023.

[6] M. Karlberg, M. Lofstrand, S. Sandberg and M. Lundin, "State of the art in simulation-driven design," International Journal of Product Development, vol. 18, no. 1, pp. 68-87, 2013.

[7] H. H. Lee, Finite Element Simulations with ANSYS Workbench 2019. Mission, KS, USA: SDC Publications, 2019.

[8] P. Kurowski, Engineering Analysis with SolidWorks Simulation 2015. Mission, KS, USA: SDC Publications, 2015.

[9] H. H. Lee, Finite Element Simulations with ANSYS Workbench 2023: Theory, Applications, Case Studies. Mission, KS, USA: SDC Publications, 2023.

[10] G. D. Manolis, P. S. Dineva, T. Rangelov and D. Sfyris, "Mechanical models and numerical simulations in nanomechanics: a review across the scales," Engineering Analysis with Boundary Elements, vol. 128, pp. 149-170, 2021.

[11] J. Stoller and B. Dubec, "Design and assessment of shape of protective structure by usage of CFD software environment Ansys Fluent," in Durability of Critical Infrastructure, Monitoring and Testing: Proc. ICDCF 2016, Singapore: Springer, 2016, pp. 200-210.

[12] X. Chen and Y. Liu, Finite Element Modelling and Simulation with ANSYS Workbench. Boca Raton, FL, USA: CRC Press, 2018.

[13] C. Harika, A. S. Kumar and M. R. Rao, "Comparative study on effect of material on structural performance of a quadcopter drone with X-frame," Journal of Physics: Conference Series, vol. 2837, no. 1, art. 012099, 2024.

[14] J. P. Veeraperumal Senthil Nathan et al., "Investigations of hybrid rotor on rotary wing UAV empennage for energy extraction and aerodynamic force enhancement," in Proc. AIAA SCITECH 2025 Forum, 2025, art. 1814.

[15] T. Barcelos and P. Fagundes-Junior, "Frugal spirals: iterative design, biomimicry, and community resilience in the Amazonian context," Journal of Sustainable Design and Innovation, vol. 12, no. 3, pp. 210-235, 2024.

[16] Yucca Manufacturing, "Annual innovation report 2023: how digital iteration cut development cycles by 40%," White Paper, 2023. [Online]. Available: https://www.yuccamfg.com/innovation-report-2023

[17] H. Zhang and Y. Wang, "A reinforcement learning framework for autonomous design iteration and fatigue optimization in additive manufacturing," in Proc. ASME 2024 Int. Design Engineering Technical Conf., 2024, paper DETC2024-117354.

[18] D. C. Tsouros, S. Bibi and P. G. Sarigiannidis, "A review on UAV-based applications for precision agriculture," Information, vol. 10, no. 11, art. 349, 2019.

[19] J. Del Cerro, C. Cruz Ulloa, A. Barrientos and J. de Leon Rivas, "Unmanned aerial vehicles in agriculture: a survey," Agronomy, vol. 11, no. 2, art. 203, 2021.

[20] C. Lee, S. Kim and B. Chu, "A survey: flight mechanism and mechanical structure of the UAV," International Journal of Precision Engineering and Manufacturing, vol. 22, no. 4, pp. 719-743, 2021.

[21] D. Van der Merwe, D. R. Burchfield, T. D. Witt, K. P. Price and A. Sharda, "Drones in agriculture," Advances in Agronomy, vol. 162, pp. 1-30, 2020.

[22] B. Stanislaus Arputharaj et al., "Comprehensive and validated computational investigations of structural integrity, aerodynamic behaviour, and its turbulence characteristics of agricultural drone with and without payload devices," Journal of Engineering, vol. 2024, art. 1386709, 2024.

[23] R. Singh, R. Kumar, A. Mishra and A. Agarwal, "Structural analysis of quadcopter frame," Materials Today: Proceedings, vol. 22, part 4, pp. 3320-3329, 2020.

[24] Raise3D, "ABS 3D printing: properties, settings, tips and steps," 2025. [Online]. Available: https://www.raise3d.com/blog/abs-3d-printing/

[25] W. An, P. Wang and H. Yang, "Study of processing parameters in fused deposition modeling based on mechanical properties of acrylonitrile-butadiene-styrene filament," Polymer Engineering and Science, vol. 59, no. 1, pp. 120-128, 2019.

[26] J. H. Park and J. Lee, "Effects of polymerization and microstructure on the printing and annealing of acrylonitrile-butadiene-styrene (ABS) for material extrusion additive manufacturing," Bulletin of the American Physical Society, 2024.

[27] J. Patil and V. Meenakshisundaram, "Structural analysis of a UAV fuselage," *International Journal of Innovative Research in Management, Engineering and Technology*, vol. 1, no. 10, Nov. 2016.

[28] J. N. Reddy, Introduction to the Finite Element Method. New York, NY, USA: McGraw-Hill, 2019.

[29] D. L. Logan, A First Course in the Finite Element Method. Boston, MA, USA: Cengage Learning, 2017.

[30] Y. Guo, X. Liu, C. Bai, J. Wang and Y. Wang, "Impact of low-altitude drop of civilian light and small UAVs on the safety of ground personnel," Aerospace Science and Technology, 2021.

Received: 06/07/2026; Revised: 22/07/2026; Accepted: 30/07/2026; Published: 15/08/2026